Organic & Biomolecular Chemistry

Cite this: *Org. Biomol. Chem.*, 2012, **10**, 8994

www.rsc.org/obc

PAPER

Absolute configuration and biological profile of two thiazinooxadiazol-3-ones with L-type calcium channel activity: a study of the structural effects

Pierfranco Ioan,[a] Alessia Ciogli,[b] Francesco Sirci,[c] Roberta Budriesi,[a] Barbara Cosimelli,[d] Marco Pierini,[b] Elda Severi,[d] Alberto Chiarini,[a] Gabriele Cruciani,[c] Francesco Gasparrini,[b] Domenico Spinelli[e] and Emanuele Carosati*[c]

Received 16th May 2012, Accepted 1st October 2012
DOI: 10.1039/c2ob25946j

In the framework of our interest in racemic thiazinooxadiazol-3-ones we determined the absolute configuration and the biological activity as L-type calcium channel blockers of two compounds that differ in the length of the acetal chain, which could affect the pharmacological profile. We observed an interesting inversion of the stereoselectivity, with the activity residing on the *R*-form for a short chain compound ($n = 1$) and on the *S*-form for a long chain one ($n = 12$). The length of the linear acetal chain appears to be able to invert the stereoselectivity of such a class of compounds, and *in silico* simulations suggested that this different behaviour might be explained by different hydrophilic and hydrophobic interactions with the binding site.

Introduction

L-Type calcium channel (LTCC) blockers are drugs approved for the treatment of cardiovascular diseases in the 1980s.[1] Their use represents a largely diffused system for monitoring the mammalian cardiac activity,[2] and has been extended to additional conditions such as the Raynaud phenomenon, pulmonary hypertension, diffuse esophageal spasm, and cerebral vasospasm[3] and as a coadjuvant in anticancer therapy, *i.e.* as inhibitors of multi-drug resistance (MDR) activity.[4,5]

The prototypical agents of LTCC blockers are: nifedipine (NIF), a member of the 1,4-dihydropyridine class (DHP); diltiazem (DTZ), a 1,5-benzothiazepinone of the benzothiazepine class (BTZ); and verapamil (VER), a member of the phenylalkylamine class (PAA). They interact at discrete receptor sites associated at the main α_1 subunit of the channel and their pharmacological effects are due to the modulation of calcium entry through the LTCC.[6]

[a]*Dipartimento di Scienze Farmaceutiche, Università degli Studi di Bologna, Via Belmeloro 6, 40126 Bologna, Italy*
[b]*Dipartimento di Chimica e Tecnologie del Farmaco, Università "La Sapienza", Piazzale A. Moro 5, 00185 Roma, Italy*
[c]*Dipartimento di Chimica, Università degli Studi di Perugia, via Elce di Sotto 10, 06123 Perugia, Italy. E-mail: emanuele@chemiome.chm.unipg.it; Fax: +39 075 45646; Tel: +39 075 585 5550*
[d]*Dipartimento di Chimica Farmaceutica e Tossicologica, Università degli Studi di Napoli "Federico II", Via Montesano 49, 80131 Napoli, Italy*
[e]*Dipartimento di Chimica 'G. Ciamician', Università di Bologna, Via Selmi 2, 40126 Bologna, Italy*

The stereoselectivity of several ligand–channel interactions is well established, including DHPs, BTZs and PAAs interacting with LTCCs;[7,8] as an example, the activity of DTZ resides almost entirely in one (2*S*,3*S*) out of its four possible diastereoisomers.[9,10] In this framework, our research group developed myocardial calcium channel modulators starting from the molecular resemblance of the chemical structure of 8-aryl-8*H*[1,4]-thiazino[3,4-*c*][1,2,4]oxadiazol-3-one derivatives with that of DTZ.[11] Incidentally, some of these compounds were also promising inhibitors of MDR1 activity.[12]

These molecules possess a chiral atom, central with respect to the molecular structure, that might affect ligand–channel interactions. The enantiomeric separation of the racemic mixture was recently carried out,[13] followed by absolute configuration determination and analysis of biological activity of the two enantiomers of the most potent compound of a series of 8-aryl-8-hydroxy-5-methyl-8*H*[1,4]thiazino[3,4-*c*][1,2,4]oxadiazol-3-ones and the corresponding 8-alkoxy derivatives, namely the 8-ethoxy derivative **1**. The *R*(−)-enantiomer was proven to be responsible for the decrease of the force of cardiac muscle contraction, showing nanomolar negative inotropic potency.[13]

Binding experiments with [^3H]diltiazem revealed a displacement of the marked probe at significantly high concentrations of **1** (10^{-4} M) whereas it was potentiating DTZ binding at low concentrations (10^{-9}–10^{-6} M). These findings indicated that these two compounds share the same binding site even if limited to high concentrations of **1**.

One hypothesis of such behaviour might be the stereoselective interaction with the channel, already known for DTZ.[9] To gain

further insight into this ligand–channel interaction we examined the thiazinooxadiazol-3-ones **2** and **3** (Chart 1), already studied as racemic mixtures.[11,14]

These two compounds were selected among those previously investigated as racemic mixtures,[11,14] and chemical and biological characteristics of the racemates guided the selection. Chemically, the nature of the substituent in the aryl moiety, the length of the acetal chain, and the calculated log *P* (2.27, 1.61, and 7.18 for **1**, **2**, and **3**, respectively) were considered: compounds **2** and **3** differ for the atom at the *para*-position of the aryl chain, chlorine for **2** and bromine for **3**; the acetal chain was of different length, ranging from one carbon atom for **2** (R = CH_3) to twelve atoms for **3** (R = *n*-$C_{12}H_{25}$), thus affecting the log *P* as well. Biologically, both chlorine for **2** and bromine for **3** (but with a particular prevalence of bromine) favourably affect the cardiovascular profile. In particular, **2** showed a negative inotropic potency two-times lower than DTZ whereas **3** six-times higher than DTZ (Table 1).[14] Notably, **3** was the most potent among the studied acetals with a long linear chain,[14] thus raising the hypothesis of a key role played by the acetal chain length.

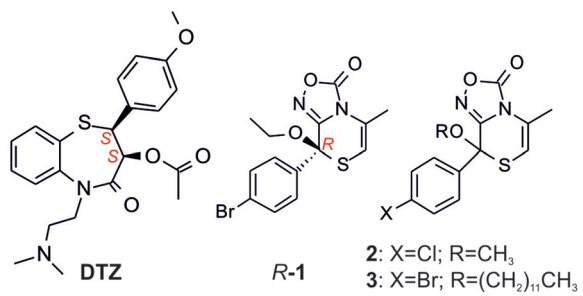

Chart 1 Structures of diltiazem (DTZ), *R*-**1**, and the two new thiazinooxadiazol-3-ones **2** and **3**.

Results and discussion

For both compounds **2** and **3** we first carried out the enantiomeric separation by using chiral chromatography, then assigned the absolute configuration by simulation of CD spectra, and finally determined the biological profile of the two enantiomers. *In silico* molecular superimpositions of the studied compounds over DTZ completed the stereoselective analysis of the ligand–channel interaction.

Conformational analysis and calculations of the electronic circular dichroism (ECD)

The pure enantiomers of **2** and **3** were obtained by semipreparative HPLC. Since the structures of **2** and **3** are strictly related to that of **1**, for which the absolute configuration was successfully elucidated through suitable comparison between experimental and theoretically calculated Electronic Circular Dichroism (ECD) and Optical Rotatory Dispersion (ORD) spectra,[13,15] we expected a very similar trend for relevant pseudoscalar properties such as optical rotation, ORD and ECD spectra. Nevertheless, we could not exclude *a priori* conformational differences and, in turn, different chiroptical properties when changing the 8-ethoxy group (**1**) with 8-methoxy (**2**) or, especially, with the significantly longer 8-dodecyloxy (**3**) ones.

Thus, in order to assign the absolute configuration to the first and second chromatographically eluted enantiomers of **2** and **3** by an unambiguous procedure, we carried out a pertinent estimation of their pseudoscalar properties without any aprioristic assumption. Fig. 1 reports the resolved peaks of **2** (a) and **3** (b), obtained by enantioselective HPLC.

Then, structures of **2** and **3** were modelled using a three-step approach. First, exhaustive conformational searches of the relevant geometries were performed through systematic (compound **2**) and stochastic MonteCarlo (compound **3**) algorithms (see the Experimental section), whose structure optimization methods

Table 1 Cardiovascular activity of tested compounds

Comp	% Decrease (M ± SEM)		EC_{50} of inotropic negative activity		Vasorelaxant activity
	Negative inotropic activity[a]	Negative chronotropic activity[b]	EC_{50} [c] (μM)	95% conf lim ($\times 10^{-6}$)	Activity[d] (M ± SEM)
DTZ	78 ± 3.5[e]	94 ± 5.6[f,g]	0.79	0.70–0.85	88 ± 2.3[h,i]
1[j]	77 ± 1.7[f]	5 ± 0.2[e]	0.04	0.03–0.05	19 ± 0.9
R(−)-**1**[k]	58 ± 3.4[f]	16 ± 0.8	0.07	0.04–0.08	11 ± 0.7[h]
S(+)-**1**[k]	47 ± 1.4[f]	15 ± 0.9			7 ± 0.3[h]
2[l]	62 ± 2.5	22 ± 1.1	1.54	1.21–1.88	14 ± 0.9
R(−)-**2**	71 ± 0.7	15 ± 1.3	0.80	0.53–1.01	35 ± 2.3
S(+)-**2**	48 ± 1.2	12 ± 0.9			21 ± 1.3
3[j]	59 ± 1.2[e]	16 ± 0.9	0.13	0.09–0.15	3 ± 0.2
R(−)-**3**	43 ± 2.1	3 ± 0.2			5 ± 0.4[m]
S(+)-**3**	67 ± 0.8[f]	10 ± 0.7	0.014	0.010–0.020	4 ± 0.1[m]

[a] Activity: decrease on developed tension in isolated guinea-pig left atrium at 5×10^{-5} M, expressed as percent changes from the control (n = 4–6). The left atria were driven at 1 Hz. The 5×10^{-5} M concentration gave the maximum effect for most compounds. [b] Activity: decrease on atrial rate in guinea-pig spontaneously beating isolated right atria at 5×10^{-5} M, expressed as percent changes from the control (n = 6–8). Pretreatment heart rate ranged from 170 to 195 beats per min. The 5×10^{-5} M concentration gave the maximum effect for most compounds. [c] Calculated from log concentration–response curves (Probit analysis according to Litchfield and Wilcoxon[17] with n = 6–8). When the maximum effect was <50%, the EC_{50} inotropic, EC_{30} chronotropic and IC_{50} values were not calculated. [d] Activity: percent inhibition of calcium-induced contraction on K^+-depolarized guinea-pig aortic strips at 5×10^{-5} M. The 5×10^{-5} M concentration gave the maximum effect for most compounds. [e] At 10^{-5} M. [f] At 10^{-6} M. [g] EC_{30} = 0.07 μM (c.l. 0.064–0.075). [h] At 10^{-4} M. [i] IC_{50} = 2.6 μM (c.l. 2.2–3.1). [j] From ref. 14. [k] From ref. 13. [l] From ref. 11. [m] At 5×10^{-6} M.

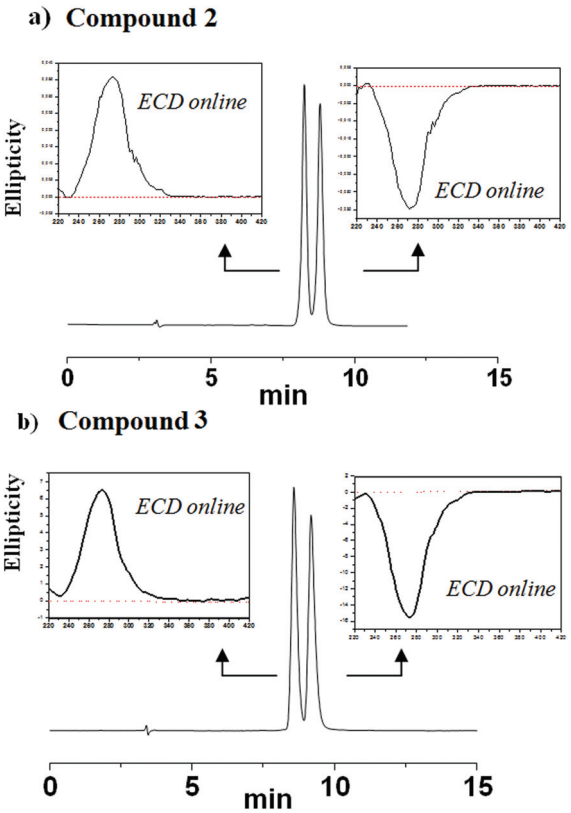

Fig. 1 Enantioselective HPLC of compounds **2** (a) and **3** (b). Chiralpak-IB column (250 × 4.6 mm I.D.), *n*-hexane–isopropanol 95 : 5, flow 1.00 mL min^{-1}, UV at 270 nm were used for **2** and (*S*,*S*)-Poly-brush-DACH-ACR column (250 × 4.6 mm I.D.), *n*-hexane–dichloromethane 85 : 15, flow 1.00 mL min^{-1} UV at 254 nm were employed for **3**. Displayed ECD spectra are recorded online.

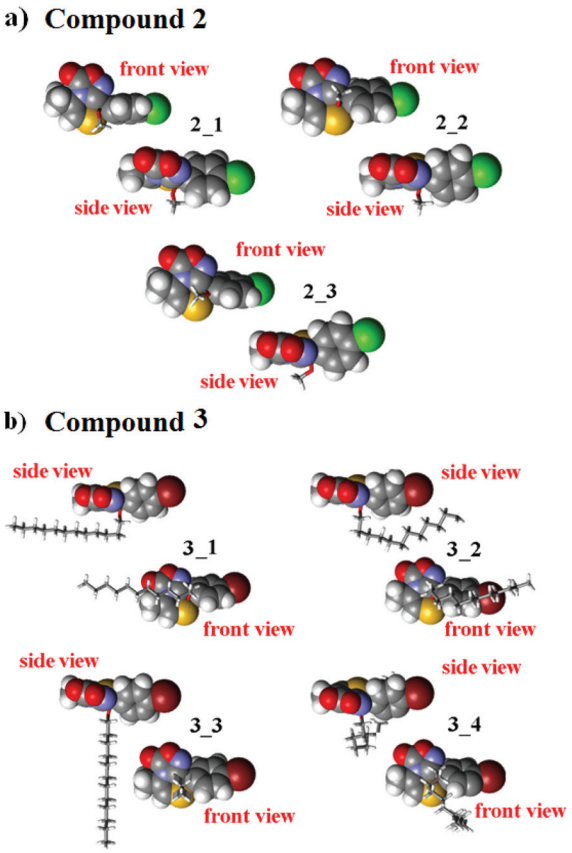

Fig. 2 Optimized conformations of compounds **2** and **3**. Structures **2_1**–**2_3** represent the only three geometries found by systematic conformational search of **2**, whereas structures **3_1**–**3_4** represent the most stable geometries within each of the four ensembles of structures found by stochastic conformational search of **3**.

were based on molecular mechanics calculations (force field: MMFF).

Secondly, the obtained conformations were ranked according to their Boltzmann population. Given the low flexibility of the methoxy group, only three conformations were used for **2**, whereas thirty conformations, within an energy window of 2 kcal mol^{-1}, were used for **3**. These conformations were grouped on the basis of the orientation assumed by the alkoxy group at position 8 with respect to both the phenyl and bicyclic ring moieties (Fig. 2).

According to the Boltzmann populations, three conformers of **2** and four among the thirty selected conformations of **3** represented a global population of 99% of the whole population of **2** and **3**, respectively. However, in order to select three conformations also for **3**, the most representative geometries (conformations **3_1**, **3_2** and **3_3**) were considered, which express 95% of the whole population.

As a third step, for these six conformers first the geometry was further optimized through the B3LYP/6-31G* DFT method, then the relevant chiroptical properties were calculated. In particular, both ECD and ORD plots were derived for each of the six optimized geometries and the final graphs, shown in Fig. 3, were achieved by merging the data plot relevant to the single conformations of **2** or **3** according to their corresponding Boltzmann populations.

The comparison of experimental and calculated ECD spectra allowed us to attribute the (*S*)-configuration to the first eluted enantiomer of both **2** and **3**. Similarly, in both cases the comparison of experimental and calculated ORD allowed us to assign the (*S*)-configuration to the dextrorotatory enantiomers (Fig. 3).

Functional results

The functional behaviour of the two enantiomers of **2** and **3** was evaluated according to a well-established protocol, already published elsewhere[16] and reported in the Experimental section. Overall, negative inotropic activity and negative chronotropic activity were evaluated on guinea-pig isolated left atria driven at 1 Hz and on spontaneously beating right atria, respectively (Table 1). In addition, calcium antagonistic activity was tested on K^+-depolarized (80 mM) guinea-pig aortic strips (Table 1) and guinea-pig ileum longitudinal smooth muscle (GPILSM) (Table 2) to assess relaxant activity on vascular and non-vascular smooth muscle, respectively.

The overall pharmacological profile of **2** and **3** was not surprising since, in line with the previous experiments conducted on the racemic mixtures, no significant vasorelaxant activity was observed for the four enantiomers (two of **2** and two of **3**) whereas a weak relaxant activity on GPILSM was observed

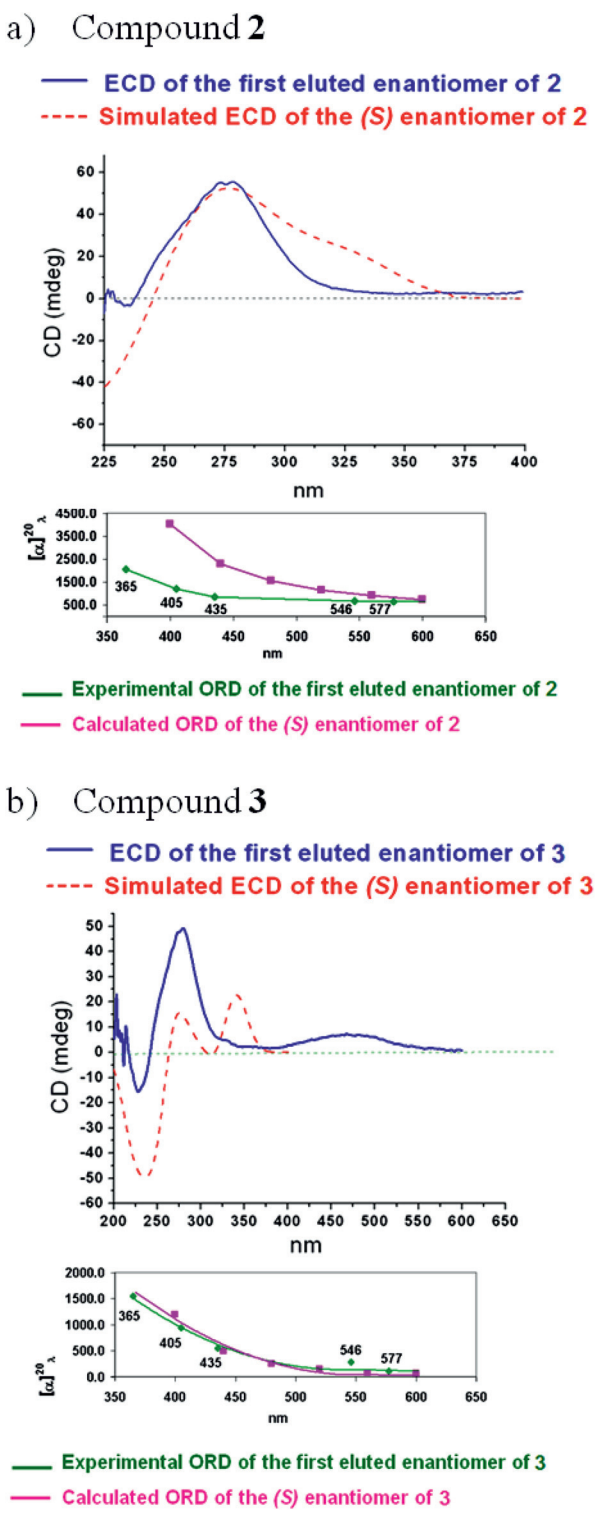

Fig. 3 Experimental and calculated ECD and ORD plots of first eluted and (*S*) enantiomers of compounds **2** (a) and **3** (b).

limited to **2**. Interestingly, for this compound activity and potency of the two enantiomers were not significantly different from those of the racemate, indicating that the non-vascular smooth muscle activity and (weak) potency are not influenced by the stereochemistry of the molecule. Conversely, a marked difference was observed for the negative inotropic activity values of the enantiomers of **2** as well as for those of **3**. In the case of the short methoxy group, at the same concentration (5×10^{-5} M) the second eluted enantiomer, namely *R*-**2**, shows an intrinsic negative inotropic activity of 71 ± 0.7, higher than that of *S*-**2**, which was 48 ± 1.2. Even more marked was the difference in the intrinsic activity of the two enantiomers of **3**, for which the value was 67 ± 0.8 at 10^{-6} M for the first eluted enantiomer (*S*-**3**), and only 43 ± 2.1 at 5×10^{-5} M for the second eluted enantiomer, namely *R*-**3**.

Table 2 Relaxant activity on K^+-depolarized guinea-pig ileum longitudinal smooth muscle

Comp	Activity[a] (M ± SEM)	IC_{50} [b] (μM)	95% conf lim ($\times 10^{-6}$)
DTZ	98 ± 1.5[c]	0.11	0.085–0.13
1[d]	3 ± 0.2		
2	61 ± 1.3	15.68	11.81–19.83
R(−)-**2**	68 ± 2.3	13.53	10.07–15.88
S(+)-**2**	65 ± 1.4	16.32	14.03–19.24
3	22 ± 0.3		

[a] Percent inhibition of calcium-induced contraction on 80 mM K^+-depolarized guinea-pig longitudinal smooth muscle at 10^{-4} M. The 10^{-4} M concentration gave the maximum effect for most compounds. [b] Calculated from log concentration–response curves (Probit analysis according to Litchfield and Wilcoxon[17] with n = 6–8). When the maximum effect was <50%, the IC_{50} values were not calculated. [c] At 10^{-6} M. [d] From ref. 13.

The most intriguing finding presented here is that the two molecules **2** and **3**, when considering the negative inotropic activity and potency, showed opposite stereoselective behaviour, with the *R*-form of **2** and the *S*-form of **3** being the eutomers. The behavior of **2**, despite its lower potency, is in line with that of the slightly flexible **1**, for which the enantioselective activity has been previously reported.[13,15] In both cases the potency has increased approximately 2-times in the more potent enantiomer. Instead, an inversion of selectivity occurs when passing from the short alkyl chains (methoxy or ethoxy) to the long, more flexible, chain of **3** (dodecyloxy). In this case, besides the displacement of activity there is also an increase of potency, with the enantiomer about 10-times more potent than the racemic mixture.

Thus, the use of computational methods, already used to hypothesize the binding mode of other calcium channel antagonists with similar or different scaffolds,[18] was invoked to shed some light on the hypothetical binding mode of these compounds. As mentioned in the introduction, this family of thiazinooxadiazolon-3-ones with calcium antagonist activity was developed bearing in mind a structural similarity with DTZ, which was first hypothesized[14] and then proved with binding experiments.[13] The intriguing results reported here, *i.e.* the inverted stereoselectivity, prompted us to look for alternative methods to explain the reasons for such different behaviour. One of the possibilities available so far is the use of a common reference framework, that would be a protein binding pocket in cases where the target three-dimensional structure is available or, as in the case of LTCC blockers, the molecular structure of a compound that shares the binding site with the molecules to be compared.

Molecular superimpositions and binding mode hypotheses

Compounds **1**, **2** and **3** were imported in the software FLAP[19] and superimposed over DTZ, which was considered as a molecular template. In this phase the choice of the conformations is aimed at determining a set of energetically stable solutions which are also diverse from each other. With respect to the previously used method (geometry optimization for calculation of ECD spectra), the method used here is based on an in-house derivation of the MM3 force-field.[20]

This procedure, detailed in the Experimental section, was applied to compounds **1**, **2** and **3**; thus, using 50 as the maximum number of diverse conformers selectable by FLAP, 20 conformers were produced for *R*-**1** as well as for *S*-**1**, 12 for **2** (both *R*- and *S*-forms), and 25 for **3** (both *R*- and *S*-forms). Molecular flexibility was considered also for the template, and for DTZ the same analysis was carried out, and 10 conformations were produced by FLAP.

Once imported, for each molecule the Molecular Interaction Fields (MIF) were generated with the GRID probes DRY, OH2 and H.[21] While the probe H simply refers to the molecular shape, the DRY and OH2 probes refer to those hydrophobic and hydrophilic regions around the molecule where favorable interactions are likely to occur with the hydrophobic and hydrophilic atoms and groups of the protein binding site, respectively. With FLAP the molecular similarity is calculated, once two molecules are superimposed, by assessing the degree of overlapping between their corresponding MIF (details are given in the Experimental section). The resulting similarity scores for the studied molecules are reported in Table 3a; these scores are in the range 0–1, and the higher the score the more similar are the two molecules. The selected orientations (discussed below and reported in Fig. 4) are those with the highest overall MIF-similarity toward DTZ (named 'Global'), obtained when superimposing the two molecules (over DTZ) using FLAP.

Fig. 5 reports the MIF for DTZ (a) and the two enantiomers of **1** (b,c), **2** (d,e) and **3** (f,g). Since the MIF of the three molecules have the same energy value, comparisons are allowed in terms of extension and relative position of such MIF points.

DTZ has a wide hydrophilic region, which is extended from the amine nitrogen to the carbonyl of the benzothiazepine ring, till the ester group. Of course, part of this region (due to N) is subjected to the flexibility of the ethylene chain, but a major change would occur in the case of inversion of configuration of one of the two carbon atoms. Nevertheless, since we used only the (2*S*,3*S*) configuration of DTZ we focus here on the intermolecular comparisons, that is comparing DTZ with the two enantiomers of **1**, **2**, or **3**.

R-**1** has a smaller (if compared to DTZ) blue-coded hydrophilic region; *S*-**1** has a hydrophilic region of the same volume of *R*-**1**, but with the orientation as in Fig. 4 its MIF only partially overlaps with those of DTZ. The DRY MIF of *S*-**1** and *R*-**1** overlap with those of DTZ to a similar extent. Thus, the most relevant difference between the two enantiomers of **1** is their molecular shape (highlighted in Table 3 as dark-gray (high relevance)), represented with the surface in Fig. 5. The *S*-form has a better fit over DTZ than the *R*-form; however, such a better fit has no direct relationship with the inotropic activity, which resides only on the *R*-form.

Table 3 Similarity scores obtained by FLAP when using DTZ as the template and **1**, **2**, and **3** as ligand-molecules (a), or DTZ as the ligand-molecule and **1**, **2**, and **3** as templates (b). The asymmetry of the scores is due to the asymmetry of the FLAP scoring functions. Symbols "∧" and "∨" are used to easily identify the enantiomers with higher scores, the percentage values are the difference between the two scores divided by the score with the higher value, whereas colored cells are used to highlight the most relevant scores: white = no relevance; light-gray = low relevance; dark-gray = high relevance. In other words, light-gray is used to mark those cells in which the difference between the scores of the two enantiomers is larger than 10%, whereas dark-gray those for which the difference is larger than 15%

(a)	H	OH2	DRY	Global
R-**1** over **DTZ**[a]	0.43	0.34	0.28	0.44
	∧ (19%)	∨ (9%)	∨ (4%)	∧ (8%)
S-**1** over **DTZ**[b]	**0.53**	0.31	0.27	0.48
R-**2** over **DTZ**[c]	0.41	**0.36**	0.29	0.44
	∧ (18%)	∨ (19%)	∧ (9%)	∧ (8%)
S-**2** over **DTZ**[d]	**0.50**	0.29	0.32	0.48
R-**3** over **DTZ**[e]	0.43	**0.32**	0.30	0.44
	∨ (7%)	∨ (22%)	∧ (12%)	∨ (5%)
S-**3** over **DTZ**[f]	0.40	0.25	**0.34**	0.42
(b)	**H**	**OH2**	**DRY**	**Global**
DTZ over *R*-**1**[a]	0.43	0.39	0.22	0.44
	∧ (17%)	∨ (3%)	∧ (8%)	∧ (10%)
DTZ over *S*-**1**[b]	**0.52**	0.38	0.24	0.49
DTZ over *R*-**2**[c]	0.42	**0.46**	0.18	0.43
	∧ (14%)	∨ (39%)	∧ (10%)	–
DTZ over *S*-**2**[d]	**0.49**	0.28	0.20	0.43
DTZ over *R*-**3**[e]	0.42	0.28	0.22	0.41
	–	∧ (46%)	∧ (24%)	∧ (13%)
DTZ over *S*-**3**[f]	0.42	**0.52**	**0.29**	**0.47**

[a] RMSD = 0.67. [b] RMSD = 0.48. [c] RMSD = 0.11. [d] RMSD = 1.20. [e] RMSD = 1.54. [f] RMSD = 1.76.

A similar analysis can be derived for the two enantiomers of **2** (Table 3a, Fig. 4c, d and 5d, e). The *R*-form has a higher hydrophilic similarity score, that could be responsible for the selective negative inotropic activity, whereas the *S*-form has a better shape-fit over DTZ, that nevertheless is not related to the activity. Both scores are dark-gray colored in Table 3. These findings let us suppose that, limited to **1** and **2**, different driving forces might guide the two enantiomers within the DTZ binding pocket, mostly hydrophilic-based in the case of *R* and mostly shape-based in the case of *S*, with therefore hydrophilicity as responsible for the stereoselectivity.

When repeating the analysis for **3** (Table 3a, Fig. 4e, f and 5f, g), the *R*-form reflects the same orientation of the previous two molecules, with the alkyl chain partially superimposed on the amine-ethylene chain of DTZ, but with a large part (at least 7 or 8 carbon atoms) completely free to move anywhere, and not

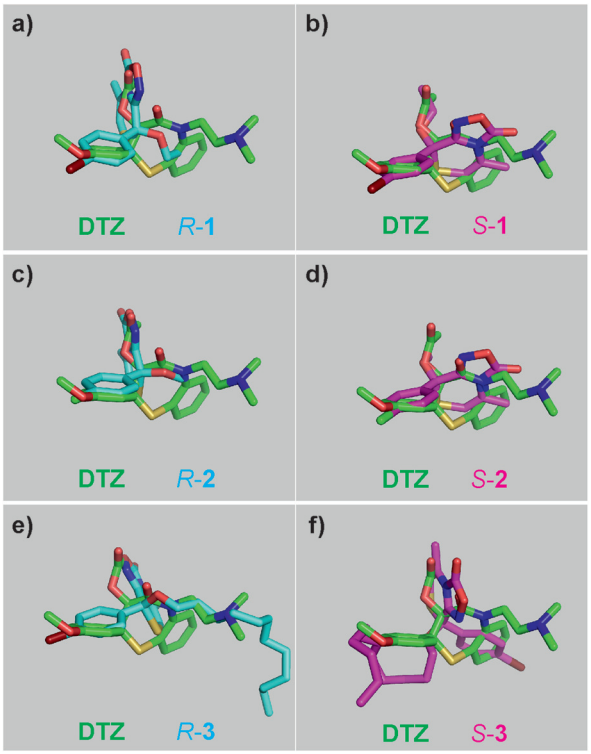

Fig. 4 Molecular superimpositions of both the enantiomers of **1**, **2**, and **3** over DTZ obtained using FLAP. Oxygen atoms are red, nitrogen atoms are blue, bromine atoms (a, b, e, f) are purple, chlorine atoms (c, d) are light-green. Carbon atoms of DTZ are green-colored, those of the *R*-form of the three molecules (**1**, **2**, and **3**) are cyan-colored, whereas those of the *S*-form are magenta-colored. Hydrogen atoms are not reported for clarity.

superimposed at all over the template. Instead, the orientation of *S*-**3** is characterized by the folding of the alkyl chain in correspondence of the *p*-methoxy-phenyl moiety of DTZ. These orientations, in terms of scores, give rise to an even larger hydrophilic score for *R*-**3** (dark-gray), a higher hydrophobic score for *S*-**3** (light-gray) and a reduced difference in terms of shape (H) for the two enantiomers (white-colored, in contrast to **1** and **2**, that are dark-gray).

Some of these findings might be related to the observed stereoselectivity; we believe that the different orientation of *S*-**3** with respect to those of *S*-**1** and *S*-**2** might represent the reason why the long chain causes the inversion of the stereoselectivity. To check this hypothesis, the ligand-based superimposition procedure was repeated, but using the six orientations of the enantiomers of **1**, **2**, and **3** as templates and the selected orientation of DTZ as the ligand molecule (without conformers generation). The collected similarity scores are reported in section b of Table 3.

Interestingly, the orientations of the ligand–template pairs obtained in this case were very close to those previously obtained, with an average root-mean-square deviation (RMSD) of 0.96, ranging from 0.11 of *R*-**2** to 1.76 of *S*-**3**. Table 3b reports the similarity scores calculated with this novel approach. Most of the findings previously observed were still valid, with the hydrophilic fields likely responsible for a better

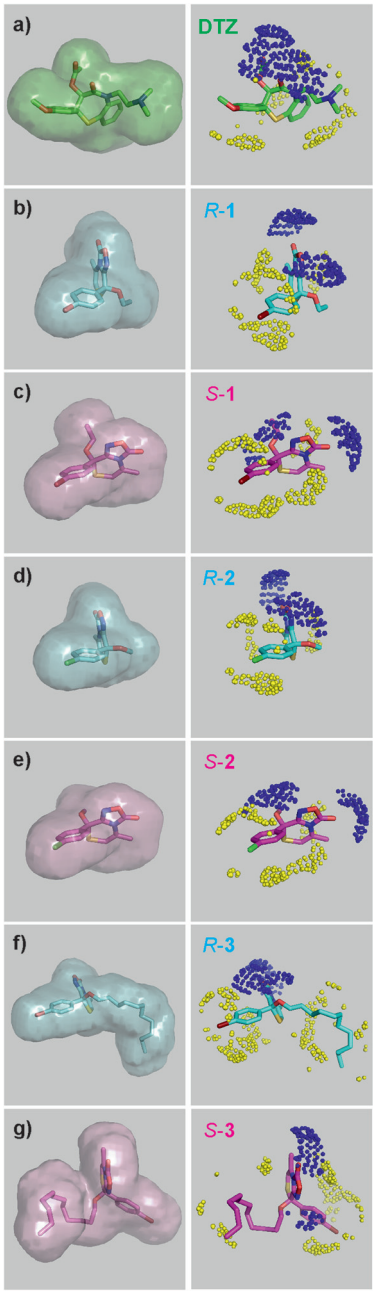

Fig. 5 MIF obtained with the GRID probes H, OH2 and DRY for DTZ (a) and the two enantiomers of **1** (b: *R*-**1**; c: *S*-**1**), **2** (d: *R*-**2**; e: *S*-**2**), and **3** (f: *R*-**3**; g: *S*-**3**). Oxygen atoms are red, nitrogen atoms are blue, bromine atoms are purple, chlorine atoms (c, d) are light-green. Carbon atoms of DTZ are green-colored, those of *R*-**1**, *R*-**2** and *R*-**3** are cyan-colored, whereas those of *S*-**1**, *S*-**2** and *S*-**3** are magenta-colored. Hydrogen atoms are not reported for clarity. The colored surface represents the isocontour corresponding to the energy values of the MIF set to +0.5 kcal mol^{-1} for the H probe. The yellow-coded spheres represent grid points where the calculated energy with the DRY probe was −0.8 kcal mol^{-1} or lower, whereas the blue spheres represent grid points where the calculated energy with the OH2 probe was −4.5 kcal mol^{-1} or lower. In the GRID force-field such a value represents, for example, the energy of the interaction between a water molecule, donating a hydrogen, with a potent heteroatom, involved as a donor, for an optimally oriented hydrogen bond interaction.

superimposition of DTZ over the *R*-forms of **1** and **2** (with respect to their corresponding *S*-forms). Concerning the similarity scores of DTZ over the two enantiomers of **3**, the major finding was a higher value observed for DTZ with *S*-**3** rather than *R*-**3** for both the hydrophilic and hydrophobic fields.

Conclusions

In this study the stereoselectivity of two new thiazinooxadiazol-3-ones with calcium antagonist activity has been studied. Enantiomeric separation using chiral chromatography, ECD spectra to assign the absolute configuration, functional studies on several guinea-pig tissues, and molecular superimpositions over DTZ have been combined to study the stereoselective behavior of the two compounds.

Experimentally, an inversion on the stereoselectivity was observed for compounds which mainly differ in the length of their alkoxy chain: the activity was residing on the *R*-form for the short chain and on the *S*-form for the long chain. Our hypothesis, based also on the fact that the thiazinooxadiazol-3-ones and DTZ share the same binding site at the LTCC, is that the hydrophilic interactions are the main driving force of the activity and, in turn, of the stereoselectivity.

The stereoselective behaviour of **1**, already described elsewhere,[13,15] has been confirmed by a similar behaviour observed for **2**, that differs from **1** for a single carbon atom (methoxy/ethoxy). The longer alkyl chain was supposed to be responsible for the inversion of the selectivity, likely due to a better fit of the chain of the *S*-form in a hypothetical hydrophobic subpocket of the LTCC binding site where the *p*-methoxy-phenyl moiety of DTZ is likely to bind.

In summary, molecular shape and hydrophilic interactions are the key factors for the inotropic activity and for the selectivity of this set of thiazinooxadiazol-3-ones.

Experimental

A. Chemistry

8-Aryl-8-alkoxy-5-methyl-8*H*[1,4]thiazino[3,4-*c*][1,2,4]oxadiazol-3-ones **2** and **3** were synthesized as previously reported.[11,14]

B. Enantiomers separation

Apparatus. Analytical liquid chromatography was performed on a JASCO chromatograph equipped with a Rheodyne model 7725i 20 µL loop injector, a PU-980 HPLC pump, a single wavelength absorbance detector Mod Jasco-975 and a circular dichroism detector Jasco Mod 995-CD. Chromatographic data were collected and processed using Borwin software (Jasco Europe, Italy). Semi-preparative liquid chromatography was performed on a Waters chromatograph (Waters Associates) equipped with a Rheodyne model 7012 500 µL loop injector, a spectrophotometer UV SpectroMonitor 4100 and a refractive index Waters R401 detector.

Chromatographic procedures. The enantiomers of **2** were collected by semipreparative HPLC using a Chiralpak-IB column (250 × 10 mm I.D.), *n*-hexane–isopropanol 95 : 5 as the eluent (flow rate 5.00 mL min^{-1} and *T* 25 °C), UV (λ = 270 nm) and RI detections. Sample **2** was dissolved in the mobile phase (35 mg, $c \approx 15$ mg mL^{-1}) and each injection was loaded with 200 µL (process yield ≈ 80%). The enantiomeric excesses were determined using the analytical Chiralpak-IB column (250 × 4.6 mm I.D.), the same mobile phase employed for the semipreparative mode at flow rate 1.00 mL min^{-1} and the UV/CD detection at 270 nm. The chromatographic steps afforded **2-first eluted** (13 mg, k = 1.78, e.e. 99.9%) and **2-second eluted** (14.5 mg, k = 2.10, α = 1.18, e.e. 96.0%) isolated samples.

The pure enantiomers of **3** were obtained by semipreparative HPLC using an (*S*,*S*)-Poly-brush-DACH-ACR[22] column (250 × 10 mm I.D.), *n*-hexane–dichloromethane 90 : 10 as the eluent (flow rate 5.00 mL min^{-1} and *T* 25 °C), UV (λ = 254 nm) and RI detections. 100 µL multiple injections of racemate (18 mg, $c \approx 30$ mg mL^{-1} in the mobile phase) afforded pure enantiomers: 7.7 mg of **3-first eluted** (k = 1.70, e.e. 97.0%) and 5.5 mg of **3-second eluted** (k = 1.99, α = 1.17, e.e. 99.0%). The enantiomeric excesses were determined using the analytical (*S*,*S*)-Poly-brush-DACH-ACR column (250 × 4.6 mm I.D.), *n*-hexane–dichloromethane 85 : 15 at 1.00 mL min^{-1} and the UV/CD detection at 254 nm.

The online ECD and UV spectra, ranging from 220–420 nm, were recorded for each enantiomer of **2** and **3** samples.

ECD measurements. ECD measurements were taken on a JASCO J-710 CD spectrometer, flushed with dry nitrogen using 10 mm path length quartz cuvettes. Measurements were taken on both enantiomers of **2** in dichloromethane solutions (6.18×10^{-5} M for **2-first eluted** and 7.60×10^{-5} M for **2-second eluted**) and on **3-second eluted** enantiomers in a 7.5×10^{-5} M dichloromethane solution; spectra were solvent subtracted.

Optical rotations measurements. Optical rotations measurements were taken on a JASCO P-1000 series polarimeter using 577, 546, 435, 405, 365 nm filters. The same enantiomeric solutions for ECD offline measurements were used. The measured values of optical rotation are given below.

Compound **2**, first eluted enantiomer: 577 nm, [α] = 645; 546 nm, [α] = 688; 435 nm, [α] = 844; 405 nm, [α] = 1207; 365 nm, [α] = 2050.

Compound **3**, first eluted enantiomer: 577 nm, [α] = 105; 546 nm, [α] = 281; 435 nm, [α] = 551; 405 nm, [α] = 936; 365 nm, [α] = 1548.

C. Molecular modelling calculations

Molecular modeling optimizations of structures were performed by using the computer program SPARTAN 04 (Wavefunction Inc., 18401 Von Karman Avenue, Suite 370, Irvine, CA 92612, USA). Conformational searches of compounds **2** and **3** were performed by molecular mechanic calculations based on the MMFF force field, according to the systematic (compound **2**) or stochastic MonteCarlo (compound **3**) algorithms implemented in SPARTAN. All rotatable bonds were varied.

Maximum energy gap from the lowest energy geometry for kept conformations: 40 kJ mol^{-1}; criterion adopted in the analysis of similarity to define conformers as duplicates: $R^2 \geq 0.9$.

Calculations supplied only three geometries for **2** (**2_1**, **2_2** and **2_3**), while thirty conformations by an energy window of 2 kcal mol^{-1} for **3**.

Due to the high number of conformers found for compound **3**, the most relevant structures were clustered. The grouping was based on disposition assumed by the dodecyloxy-framework with respect to the bicyclic and phenyl moieties of the molecule. From this kind of analysis four typologies of conformations were identified, corresponding to the following geometric properties: type (1) conformers with the hydrocarbon chain folded on the left of the middle position of the molecule, over the bicyclic framework (**3_1** the most stable among these structures); type (2) conformers with the hydrocarbon chain folded on the right of the middle position of the molecule, over the phenyl moiety (**3_2** the most stable among these structures); type (3) conformers with a stretched hydrocarbon chain pointing away from both bicyclic and phenyl frameworks (**3_3** the most stable among these structures); type (4) conformers with the hydrocarbon chain folded between the bicyclic and phenyl frameworks, from both the possible sides (**3_4** the most stable among these structures).

All the three geometries achieved for compounds **2** were further optimized at the SCF level by the DFT B3LYP/6-31G* method. Instead, due to the little abundance assessed for conformations type 4 of compound **3** (4% their cumulative Boltzmann Population, BP, from the molecular mechanics calculations), only the most stable ones of type 1–3 of this molecule (*i.e.*, structures **3_1**, **3_2** and **3_3**) were submitted to the same DFT optimization performed on **2**. The found relative energy amounts (E_{rel}, in kcal mol^{-1}) and BP at 25 °C of the **2_x** conformations (with *x* varying from 1 to 3) were: E_{rel} 0.00, BP 60.9%; E_{rel} 0.31, BP 36.3%; E_{rel} 1.81, BP 2.9%. For the **3_x** conformations (with *x* varying from 1 to 3) the same quantities were: E_{rel} 2.85, BP 0.8%; E_{rel} 1.79, BP 4.6%; E_{rel} 0.00, BP 94.6%, respectively. After this refinement structures were subjected to the assessment of the relevant chiroptical properties, carried out using the BLYP method with the QZ4P large core basis set for **2** and with the TZ2P large core basis set for **3**, as implemented in the Amsterdam Density Functional (ADF) package v. 2007.01. The set options were: single point calculation; 40 singlet and triplet excitations; diagonalization method: Davidson; optical rotation: 6 frequencies, from 4000.0 to 6000.0 Å. The calculated values of optical rotation are given below.

Compound **2**, first eluted enantiomer: 600 nm, [α] = 726; 560 nm, [α] = 900; 520 nm, [α] = 1155; 480 nm, [α] = 1564; 440 nm, [α] = 2307; 400 nm, [α] = 4041.

Compound **3**, first eluted enantiomer: 600 nm, [α] = 67; 560 nm, [α] = 95; 520 nm, [α] = 149; 480 nm, [α] = 253; 440 nm, [α] = 485; 400 nm, [α] = 1188.

D. Functional assays

The pharmacological profile of all compounds was tested on guinea-pig isolated left and right atria to evaluate their inotropic and chronotropic effects, respectively, and on K^+-depolarized guinea-pig aortic strips and guinea-pig longitudinal smooth muscle of ileum to assess calcium antagonist activity. Compounds were checked at increasing concentrations in order to evaluate the percentage decrease of developed tension on an isolated left atrium driven at 1 Hz (negative inotropic activity), the percentage decrease in atrial rate on a spontaneously beating right atrium (negative chronotropic activity) and the percentage inhibition of calcium-induced contraction on K^+-depolarized aortic strips (vasorelaxant activity) and GPILSM (non-vascular smooth muscle relaxant activity).

Data were analyzed using Student's *t*-test. The potency of drugs defined as EC_{50}, EC_{30} and IC_{50} was evaluated from log concentration–response curves (Probit analysis using Litchfield and Wilcoxon or GraphPad Prism® software)[17,23] in the appropriate pharmacological preparations. All data are presented as mean ± SEM.

Guinea-pig atrial preparations. Female guinea-pigs (300–400 g) were sacrificed by cervical dislocation. After thoracotomy the heart was immediately removed and washed by perfusion through the aorta with an oxygenated Tyrode solution of the following composition (mM): 136.9 NaCl, 5.4 KCl, 2.5 $CaCl_2$, 1.0 $MgCl_2$, 0.4 $NaH_2PO_4{\cdot}H_2O$, 11.9 $NaHCO_3$ and 5.5 glucose. The physiological salt solution (PSS) was buffered at pH 7.4 by saturation with 95% O_2–5% CO_2 gas, and the temperature was maintained at 35 °C. The following isolated guinea-pig heart preparations were used: spontaneously beating right atria and left atria driven at 1 Hz. For each preparation, the entire left and right atria were dissected from the ventricles, cleaned of excess tissue, hung vertically in a 15 mL organ bath containing the PSS continuously bubbled with 95% O_2–5% CO_2 gas at 35 °C, pH 7.4. The contractile activity was recorded isometrically by means of a force transducer (FT 0.3, Grass Instruments Corporation, Quincy, MA, USA) using Power Lab® software (AD-Instruments Pty Ltd, Castle Hill, Australia). The left atria were stimulated by rectangular pulses of 0.6–0.8 ms duration and about 50% threshold voltage through two platinum contact electrodes in the lower holding clamp (Grass S88 Stimulator). The right atrium was in spontaneous activity. After the tissue was beating for several minutes, a length–tension curve was obtained and the muscle was stretched to the length at which 90% of maximal force was developed. A stabilization period of 45–60 min was allowed before the atria were challenged by various agents. During the equilibration period, the bathing solution was changed every 15 min and the threshold voltage was ascertained for the left atria. Atrial muscle preparations were used to examine the inotropic and chronotropic activity of the compounds (0.01, 0.05, 0.1, 0.5, 1, 5, 10, 50 and 100 μM), first dissolved in DMSO and then diluted with PSS. According to this procedure, the concentration of DMSO in the bath solution never exceeded 0.3%, a concentration which did not produce appreciable inotropic and chronotropic effects. During the generation of cumulative concentration–response curves, the next higher concentration of the compounds was added only after the preparation reached a steady state.

Guinea-pig aortic strips and ileum longitudinal smooth muscle (GPILSM). The thoracic aorta and ileum were removed and placed in a Tyrode solution of the following composition (mM): 118 NaCl, 4.75 KCl, 2.54 $CaCl_2$, 1.20 $MgSO_4$, 1.19 KH_2PO_4, 25 $NaHCO_3$ and 11 glucose equilibrated with 95% O_2–5% CO_2 gas at pH 7.4. The vessel was cleaned of

extraneous connective tissue. Two helicoidal strips (10 mm × 1 mm) were cut from each aorta beginning from the end most proximal to the heart. Vascular strips were then tied with surgical thread (6-0) and suspended in a jacketed tissue bath (15 mL) containing aerated PSS at 35 °C. Aortic strips were secured at one end to plexiglass hooks and connected *via* the surgical thread to a force displacement transducer (FT 0.3, Grass Instruments Corporation) for monitoring changes in isometric contraction. Aortic strips were subjected to a resting force of 1 g. The intestine was removed above the ileo-caecal junction. GPILSM segments of 2 cm length were mounted under a resting tension of 300–400 mg. Strips were secured at one end to a force displacement transducer (FT 0.3, Grass Instruments Corporation) for monitoring changes in isometric contraction and washed every 20 min with fresh PSS for 1 h. After the equilibration period, guinea-pig aortic strips were contracted by washing in PSS containing 80 mM KCl (equimolar substitution of K^+ for Na^+). When the contraction reached a plateau (about 45 min) various concentrations of the compounds (0.1, 0.5, 1, 5, 10, 50, 100 and 500 μM) were added cumulatively to the bath allowing for any relaxation to obtain an equilibrated level of force. Addition of the drug vehicle had no appreciable effect on K^+-induced contraction (DMSO for all compounds).

E. Molecular superimpositions

The program FLAP (Fingerprints for Ligands And Proteins) was originally conceived as a fast algorithm for performing virtual screening by means of a fingerprint-type description of both ligands and protein binding sites according to their GRID Molecular Interaction Fields.[19] It was designed to describe molecules and protein structures in terms of a common reference framework. In ligand-based virtual screening, compounds from virtual libraries are ranked according to their similarity toward a given reference molecule, called a template. Given the 3D structure of a molecule, with the GRID force-field[21] the interaction energies between the molecule and a probe are calculated at different points in space. As a result, one has the so-called Molecular Interaction Fields (MIF): the hydrophobic and hydrogen bonding interactions of the molecule with a virtual receptor are schematised by the probes and encoded into energy values assigned to the nodes of a grid built around each molecule. The core of the FLAP process is finding the matches of the four hotspots of the individual ligands to those of the template. When four hotspots (quadruplets) of the ligand molecule are found to fit over four hotspots of the template framework, a potentially favourable superposition has been detected. The process is iterative and, when executed exhaustively (maximum precision corresponds to minimum speed), it continues until all the template quadruplets are combined in all possible ways with all ligand quadruplets; in cases of faster screening, a quadruplet sampling is carried out in both the sets of the template and of each ligand molecule. For each superposition, a score associated to the two molecules and their common quadruplet of hotspots quantifies the overlap of the two MIFs: a score is assigned to the superposition in order to evaluate its "goodness" of MIF-overlapping. At the end of the process, several superpositions of each ligand to each template are memorized. Thus, compounds from virtual libraries are ranked according to their similarity toward the template. In this paper we observed a difference among the scores obtained for corresponding template-candidate alignments due to the intrinsic asymmetry of the FLAP scoring functions, as we briefly reported in the caption of Table 3. This asymmetry is due to different reasons. The first reason concerns the nature of the GRID Molecular Interaction Fields (MIF), that are a collection of float numbers assigned to each node of the grid and reporting the interaction energy between the molecule and the probe. In FLAP, once two molecules are aligned, the MIF intersection is used for the evaluation of molecular similarity. Thus, since it is highly probable that when aligning the molecules their MIF points are not aligned, a set of smoothing functions are applied to this discrete system in order to allow the evaluation of the GRID energy for the two aligned molecules in the same points of the space. It implies that some small differences may occur because of this discrete-to-continuous conversion. The second reason is the speed of the FLAP screening calculation; we set up the speed screening to 75%, that implies a sampling of the quadruplets that are used for the molecular superpositions. In our case the sampling was performed by a random selection of 1/6 of the overall amount of quadruplets of both template and candidate. However, even an exhaustive use of all the possible quadruplets may not result in the equivalence of the scores, because of the first reason.

Some details of the FLAP calculations are briefly listed: (1) The conformers are produced by FLAP on-the-fly with a routine that randomly modifies the molecule and adds a new conformation to the set only when it differs from the ones already existing. First, a random search is performed using 40 samples for each rotatable bond; this produces thousands of potential conformers, which are minimized and retained only if within an energy window of 20 kcal mol^{-1} from the minimum. Such conformers are then ranked by energy and filtered according to their diversity to the dataset, *i.e.* exclusion regards those conformers with low calculated RMSD with respect to any of the other low-energy conformers already selected. For the template DTZ the conformational analysis produced 10 different conformations, whereas 20, 12, and 25 conformers were generated for the ligand molecules **1**, **2**, and **3**, respectively. (2) GRID probes H, OH2 and DRY were used. (3) The level of speed was set to 75%.

Acknowledgements

Supported by grants from University of Bologna, and from Istituto Nazionale per le Ricerche Cardiovascolari (INRC), Italy. We thank Dr M. Baroni (Molecular Discovery Ltd, UK) for valuable discussion on the FLAP algorithm, Dr F. Fusi and Dr M. Frosini (University of Siena, Italy) for helpful discussion on the pharmacological activity of this series of LTCC blockers, and A. Casoni (University of Bologna, Italy) for animal care.

Notes and references

1 P. D. Henry, *Am. J. Cardiol.*, 1980, **46**, 1047–1058.
2 D. J. Triggle, *Biochem. Pharmacol.*, 2007, **74**, 1–9.
3 E. Grossman and F. H. Messerli, *Prog. Cardiovasc. Dis.*, 2004, **47**, 34–57.
4 M. Dean, T. Fojo and S. Bates, *Nat. Rev. Cancer*, 2005, **5**, 275–284.

5 A. Aszalos, *Drug Discovery Today*, 2007, **12**, 838–843.
6 W. G. Nayler and P. Poole-Wilson, *Basic Res. Cardiol.*, 1981, **76**, 1–15.
7 Y. W. Kwon and D. J. Triggle, *Chirality*, 1991, **3**, 393–404.
8 D. J. Triggle, *Drug Discovery Today*, 1997, **2**, 138–147.
9 T. Tanaka, H. Inoue, T. Date, K. Okamura, K. Aoe, M. Takeda, H. Kugita, S. Murata, T. Yamaguchi, K. Kikkawa, S. Nakajima and T. Nagao, *Chem. Pharm. Bull. (Tokyo)*, 1992, **40**, 1476–1480.
10 R. Budriesi, B. Cosimelli, P. Ioan, E. Carosati, M. P. Ugenti and R. Spisani, *Curr. Med. Chem.*, 2007, **14**, 279–287.
11 R. Budriesi, B. Cosimelli, P. Ioan, C. Z. Lanza, D. Spinelli and A. Chiarini, *J. Med. Chem.*, 2002, **45**, 3475–3481.
12 (*a*) M. Viale, C. Cordazzo, B. Cosimelli, D. de Totero, P. Castagnola, C. Aiello, E. Severi, G. Petrillo, M. Cianfriglia and D. Spinelli, *J. Med. Chem.*, 2009, **52**, 259–266; M. Viale, *et al*., *SciBX*, **2**(2), DOI: 10.1038/scibx.2009.44; (*b*) M. Viale, C. Cordazzo, D. de Totero, R. Budriesi, C. Rosano, A. Leoni, P. Ioan, C. Aiello, M. Croce, A. Andreani, M. Rambaldi, P. Russo, A. Chiarini and D. Spinelli, *Invest. New Drugs*, 2011, **29**, 98–109.
13 E. Carosati, G. Cruciani, A. Chiarini, R. Budriesi, P. Ioan, R. Spisani, D. Spinelli, B. Cosimelli, F. Fusi, M. Frosini, R. Matucci, F. Gasparrini, A. Ciogli, P. J. Stephens and F. J. Devlin, *J. Med. Chem.*, 2006, **49**, 5206–5216.
14 R. Budriesi, E. Carosati, A. Chiarini, B. Cosimelli, G. Cruciani, P. Ioan, D. Spinelli and R. Spisani, *J. Med. Chem.*, 2005, **48**, 2445–2456.
15 P. J. Stephens, F. J. Devlin, F. Gasparrini, A. Ciogli, D. Spinelli and B. Cosimelli, *J. Org. Chem.*, 2007, **72**, 4707–4715.
16 R. Budriesi, P. Ioan, A. Leoni, N. Pedemonte, A. Locatelli, M. Micucci, A. Chiarini and L. J. Galietta, *J. Med. Chem.*, 2011, **54**, 3885–3094.
17 R. J. Tallarida and R. B. Murray, *Manual of Pharmacologic Calculations with Computer Programs*, Springer-Verlag, New York, 2nd edn, 1987.
18 (*a*) R. Budriesi, B. Cosimelli, P. Ioan, M. P. Ugenti, E. Carosati, M. Frosini, F. Fusi, R. Spisani, S. Saponara, G. Cruciani, E. Novellino, D. Spinelli and A. Chiarini, *J. Med. Chem.*, 2009, **52**, 2352–2362; (*b*) E. Carosati, R. Budriesi, P. Ioan, G. Cruciani, F. Fusi, M. Frosini, S. Saponara, F. Gasparrini, A. Ciogli, P. J. Stephens, F. J. Devlin, D. Spinelli and A. Chiarini, *J. Med. Chem.*, 2009, **52**, 6637–6648.
19 (*a*) M. Baroni, G. Cruciani, S. Sciabola, F. Perruccio and J. S. Mason, *J. Chem. Inf. Model.*, 2007, **47**, 279–294; (*b*) S. Cross, M. Baroni, E. Carosati, P. Benedetti and S. Clementi, *J. Chem. Inf. Model.*, 2010, **50**, 1442–1450.
20 N. L. Allinger, Y. H. Yuh and J.-H. Lii, *J. Am. Chem. Soc.*, 1989, **111**, 8551–8566.
21 P. J. Goodford, *J. Med. Chem.*, 1985, **28**, 849–857.
22 (*a*) F. Gasparrini, D. Misiti, R. Rompietti and C. Villani, *J. Chromatogr., A*, 2005, **1064**, 25–38; (*b*) A. Cavazzini, F. Dondi, S. Marmai, E. Minghini, A. Massi, C. Villani, R. Rompietti and F. Gasparrini, *Anal. Chem.*, 2005, **77**, 3113–3122; (*c*) A. Ciogli, I. D'Acquarica, F. Gasparrini, C. Molinaro, R. Rompietti, P. Simone, C. Villani and G. Zappia, *J. Sep. Sci.*, 2010, **33**, 3022–3032.
23 (*a*) H. Motulsky and A. Christopoulos, 2003; (*b*) H. Motulsky, 2003; (*c*) http://www.GraphPad.com